JOURNAL OF CHEMICAL INFORMATION AND MODELING

Article

pubs.acs.org/jcim

Structure and Properties of the Nonface-Spiral Fullerenes T-C_{380}, D_3-C_{384}, D_3-C_{440}, and D_3-C_{672} and Their Halma and Leapfrog Transforms

Lukas N. Wirz,[†] Ralf Tonner,[‡] James Avery,[§] and Peter Schwerdtfeger*[,†,‡]

[†]Centre for Theoretical Chemistry and Physics, The New Zealand Institute for Advanced Study, Massey University Auckland, Private Bag 102904, 0745 Auckland, New Zealand

[‡]Fachbereich Chemie, Philipps-Universität Marburg, Hans-Meerwein-Str., D-35032 Marburg, Germany

[§]Niels Bohr Institute, University of Copenhagen, 2100 Copenhagen, Denmark

ABSTRACT: The structure and properties of the three smallest nonface-spiral (NS) fullerenes NS-T-C_{380}, NS-D_3-C_{384}, NS-D_3-C_{440}, and the first isolated pentagon NS-fullerene, NS-D_3-C_{672}, are investigated in detail. They are constructed by either a generalized face-spiral algorithm or by vertex insertions followed by a force-field optimization using the recently introduced program *Fullerene*. The obtained structures were then further optimized at the density functional level of theory and their stability analyzed with reference to I_h-C_{60}. The large number of hexagons results in a higher stability of the NS-fullerenes compared to C_{60}, but, as expected, in a lower stability than most stable isomers. None of the many investigated halma transforms on nonspiral fullerenes, NS-T-C_{380}, NS-D_3-C_{384}, NS-D_3-C_{440}, and NS-D_3-C_{672}, admit any spirals, and we conjecture that all halma transforms of NS-fullerenes belong to the class of NS-fullerenes. A similar result was found to not hold for the related leapfrog transformation. We also show that the first known NS-fullerene with isolated pentagons, NS-D_3-C_{672}, is a halma transform of D_3-C_{168}.

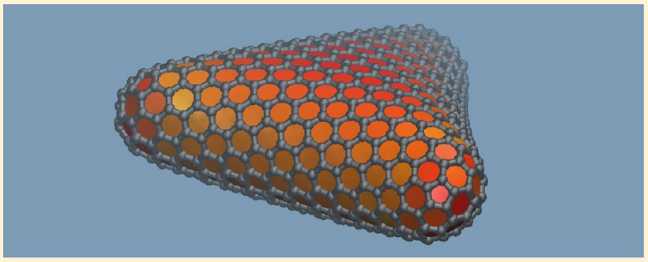

INTRODUCTION

Fullerenes have exactly 12 pentagons, and the location of the pentagons within the network of hexagons uniquely determines the fullerene structure. A convenient way to characterize fullerenes is by using the face-spiral algorithm by Manolopoulos and Fowler (MF).[1,2] This algorithm spirally unwinds (clockwise or anti-clockwise) the faces of a fullerene polyhedron into a string of pentagons and hexagons, and the locations of pentagons in that sequence result in the 12 ring- (or face-) spiral pentagon indices (RSPI) that uniquely determine the fullerene graph G_F up to isomorphism. The RSPI is thus a compact, unique, and canonical representation of fullerene isomers, from which their graphs can easily be constructed.

The success of the MF face-spiral algorithm made it tempting to conclude that every fullerene can be constructed in this manner because it holds true for the first many million isomers.[1,2] However, this is not so. Manolopoulos and Fowler found the first counterexample in 1993, showing the existence of a T-C_{380} fullerene isomer that cannot be constructed from a face spiral.[3] We call such fullerenes *nonface-spiral* or simply *nonspiral* (NS) fullerenes in the following. It appears that nonspiral fullerenes are exceedingly rare. The first two nonspiral fullerenes are T-C_{380} and D_3-C_{384},[3−5] which are shown in Figures 1 and 2. In fact, Brinkmann et al. demonstrated that these are the only two NS-fullerenes out of 2,653,606,256,199 fullerenes with 400 atoms or less.[6−8]

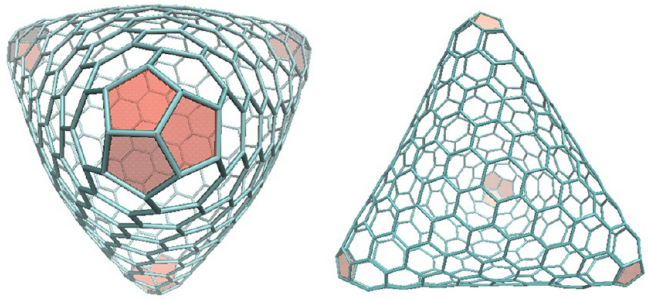

Figure 1. Density functional (B3LYP) optimized structure of the NS-fullerene T-C_{380}. View from the top (left) and side (right) of the polyhedron.

Hence, it is advantageous to identify fullerenes with their canonical face spiral and to treat the very rare fullerenes that do not have one separately.

We recently introduced a comprehensive software package called *Fullerene*, which is a general purpose program for automatically constructing, transforming, and analyzing fullerenes.[9] The program allows constructing any fullerene (whether or not it has a face spiral) from generalized ring spiral indices by way of a new algorithm and analyzing

Received: September 27, 2013
Published: December 6, 2013

   dx.doi.org/10.1021/ci4005578 | *J. Chem. Inf. Model.* 2014, 54, 121−130

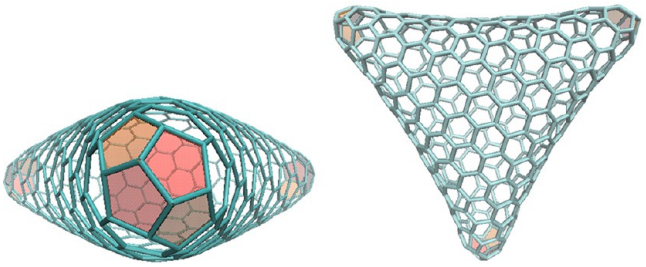

Figure 2. Density functional (B3LYP) optimized structure of the NS-fullerene D_3-C_{384}. View from the top (left) and side (right) of the polyhedron.

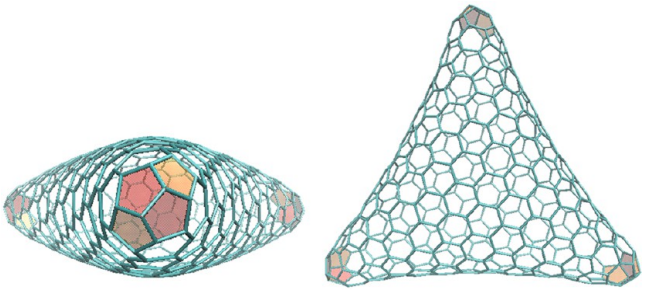

Figure 3. Density functional (B3LYP) optimized structure of the NS-fullerene, D_3-C_{440}. View from the top (left) and side (right) of the polyhedron.

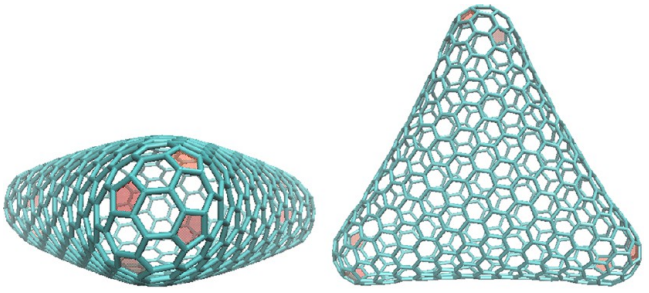

Figure 4. Density functional (B3LYP) optimized structure of the NS-fullerene, D_3-C_{672}. View from the top (left) and side (right) of the polyhedron.

topological as well as chemical properties. It produces good approximations to the molecular structures by way of force-field optimization, resulting in geometries that are close to those calculated by a much more demanding quantum theoretical treatment.

The aim of this study was to investigate the structure and topology of the smallest three NS-fullerenes, T-C_{380}, D_3-C_{384}, and D_3-C_{440}, as well as the smallest known NS-fullerene with no adjacent pentagons, D_3-C_{672}, using density functional theory (DFT) in order to obtain accurate structural properties. We further aim to study the leapfrog and halma transforms of T-C_{380}, D_3-C_{384}, D_3-C_{440}, and D_3-C_{672}, which are special cases of Goldberg−Coxeter transformations,[10,11] to highlight some important mathematical properties for this class of NS-fullerenes.

Methods. Our program, *Fullerene*,[9] first creates the fullerene graph G_F for each fullerene considered, applying the algorithms as discussed in the next section. The fullerene graph is an undirected, planar, cubic, and connected graph describing the C−C bonds, which uniquely determines a particular fullerene up to inversion. Pairs of enantiomers share the same underlying graph. All four investigated fullerenes as well as the derived structures are chiral, but as electronic and geometric properties are independent of inversion, we do not distinguish between the enantiomers. To generate the three-dimensional molecular structure, the program uses the Tutte embedding algorithm[12] to compute a planar layout of G_F, which is then projected onto a sphere to produce a 3D surface structure without crossing edges. This initial structure is then subjected to a force-field optimization specifically designed for fullerenes as described in detail in ref 9.

The force-field optimized structures were taken as input for a refined density functional theory (DFT) optimization, using the gradient corrected Perdew−Burke−Ernzerhof (PBE)[13] functional and the hybrid Becke−Lee−Yang−Parr (B3LYP)[14,15] functional together with a def2-SVP basis set[16] and the resolution of identity (RI) approximation.[17] Energies and gradients were obtained with the Turbomole and Gaussian09 program packages.[18,19] Convergence criteria were tightened with respect to the standard values (SCF convergence $<10^{-10}$ a.u., root-mean-square force $<10^{-5}$ a.u., and fine grid for the numerical integration). The optimized structures of T-C_{380} and D_3-C_{384} are shown in Figures 1 and 2. The next NS-fullerene, D_3-C_{440}, which is similar in shape compared to D_3-C_{384}, is shown in Figure 3. The first NS-fullerene with isolated pentagons is D_3-C_{672} and is shown in Figure 4. We note that the force-field implemented in *Fullerene* gives very good initial structures, e.g., the root-mean-square error in the force-field optimized bond distances is ≈0.12 Å compared to the PBE optimized structure.

For each of the four NS-fullerenes, we performed Goldberg−Coxeter (GC) transformations[10,11] $T^{GC}_{k,l}(G_F)$ for the special cases $k = l$, and for $l = 0$, in order to investigate whether or not these fullerenes can be unwound into a face spiral. We considered GC-transformed fullerenes up to $k = 7$ for $l = 0$, and to $k = 4$ for $k = l$. These very large structures, comprised of thousands of atoms, were not subjected to DFT optimizations because of the excessive computer time required but only to force-field optimizations.

In addition, we carried out B3LYP optimizations for the most stable isomer for a series of C_N structures in the range $20 \le N \le 540$ to compare to the stability of the NS-fullerenes. Here, we used an augmented correlation consistent PVDZ basis set for $20 \le N \le 60$, a correlation consistent PVDZ basis set for $60 \le N \le 180$, and a 6-31G basis set[19] for the larger fullerenes with $240 \le N \le 540$.

RESULTS AND DISCUSSION

Construction of T-C_{380} from T-C_{364} and D_3-C_{384} from D_3-C_{366} through Vertex Insertions. The concept of vertex insertions or deletions and formal isomerizations has proven to be useful, as it allows for the stepwise derivation of one fullerene graph from another.[20,21] In particular, fullerene graphs that fail to be constructed using the MF face-spiral algorithm, can be derived from smaller fullerenes that admit a spiral by vertex insertions.

Any patch of hexagons and pentagons can be characterized by its boundary code.[21,22] Any two such patches that are equal in their boundary code can be exchanged for each other. Furthermore, if the symmetry of the boundary code is higher than the symmetry of the patch itself, the patch can be replaced by a rotated instance of itself. The smallest example of such a

dx.doi.org/10.1021/ci4005578 | J. Chem. Inf. Model. 2014, 54, 121−130

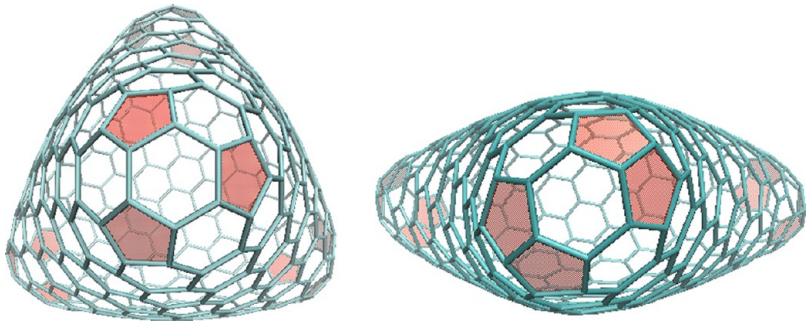

Figure 5. Density functional (B3LYP) optimized structures of T-C_{364} (left) and D_3-C_{366} (right) showing the pentagons involved in the Yoshida–Fowler four-vertex and Brinkmann–Fowler six-vertex insertions.

Table 1. Point Group Symmetry (PGS), Number of Vertices n_v, and Canonical Ring (Face) Spiral Pentagon Indices (RSPI) for Selected Fullerenes[a]

PGS	n_v	RSPI										
		T-C_{364}, C_3-C_{368}, C_2-C_{372}, C_3-C_{376}, and $T^{GC}_{k,l}[T\text{-}C_{364}]$										
T	364	12	14	27	78	101	103	118	120	143	156	172	174
C_3	368	12	14	27	78	101	103	118	120	143	173	174	186
C_2	372	12	14	27	78	101	103	119	143	144	175	176	188
C_3	376	13	27	28	80	103	105	121	145	146	177	178	190
T	1092	155	158	187	216	219	232	299	331	361	533	536	547
T	1456	155	219	254	288	324	328	362	402	453	706	717	730
T	3276	375	472	602	654	708	714	849	909	986	1583	1618	1637
T	4368	696	722	728	784	848	854	1270	1302	1426	2153	2159	2166
T	5824	691	821	1098	1168	1240	1248	1540	1620	1723	2810	2881	2906
T	9100	1103	1266	1742	1830	1920	1930	2435	2535	2664	4387	4506	4537
T	9828	1611	1620	1713	1800	1809	1848	2913	3009	3103	4844	4853	4888
T	13104	1611	1807	2534	2640	2748	2760	3534	3654	3809	6314	6493	6530
T	17836	2215	2444	3474	3598	3724	3738	4837	4977	5158	8591	8842	8885
T	17472	2915	2927	3052	3168	3180	3232	5228	5356	5482	8624	8636	8683
		D_3-C_{366}, C_2-C_{372}, C_2-C_{378}, and $T^{GC}_{k,l}[D_3\text{-}C_{366}]$										
D_3	366	1	2	14	15	140	141	164	166	177	178	183	185
C_2	372	1	2	14	15	140	141	164	166	184	185	186	188
C_2	378	1	3	4	5	143	144	167	169	187	188	189	191
D_3	1098	1	7	21	34	429	432	471	475	493	532	536	547
D_3	1464	13	15	95	97	519	521	617	661	703	705	728	732
D_3	3294	9	25	149	152	1228	1231	1444	1450	1580	1583	1637	1643
D_3	4392	1	37	91	150	1746	1752	1876	1918	1926	2043	2156	2190
D_3	5856	111	115	401	532	2063	2067	2451	2726	2808	2812	2910	2918
D_3	9150	41	71	475	480	3396	3401	3996	4006	4387	4392	4547	4557
D_3	13176	195	201	879	1068	4717	4723	5587	6001	6317	6323	6548	6560
D_3	17934	97	141	985	992	6644	6651	7820	7834	8598	8605	8913	8927
D_3	9882	1	79	193	325	3850	3859	4234	4246	4300	4666	4834	4919
D_3	17568	1	153	357	599	6911	6923	7515	7599	7615	8181	8614	8754
		$T^{GC}_{k,l}[D_3\text{-}C_{384}]$										
D_3	1152	1	11	13	24	453	496	498	542	563	572	574	577
D_3	4608	51	108	112	272	1746	1921	2005	2096	2246	2284	2288	2304
D_3	10368	51	186	192	449	4036	4426	4432	4825	5051	5138	5144	5183
		$T^{GC}_{k,l}[D_3\text{-}C_{440}]$										
D_3	1320	14	28	30	70	516	562	564	611	647	656	658	661
		D_3-C_{168} and $T^{GC}_{k,l}[D_3\text{-}C_{672}]$										
D_3	168	4	5	13	14	58	59	74	75	82	83	84	86
D_3	2016	1	41	45	90	711	763	825	849	877	954	958	1008
D_3	8064	1	161	169	351	2893	2997	3345	3393	3449	3815	3823	4030
D_3	18144	1	361	373	784	6547	6703	7561	7633	7717	8584	8596	9068
D_3	32256	1	641	657	1389	11673	11881	13473	13569	13681	15261	15277	16122

[a] $T^{GC}_{k,l}[C_n]$ denotes the two-index Goldberg–Coxeter transform of fullerene C_n.

rotation is the Stone–Wales transformation.[23] Two patches with the same boundary code must have the same number of pentagons in order to keep the number of pentagons exactly at 12 in the overall fullerene graph, as required by Euler's

dx.doi.org/10.1021/ci4005578 | J. Chem. Inf. Model. 2014, 54, 121–130

Table 2. Goldberg–Coxeter Indices (k,l), Triangulation Parameter $t(k,l)$, Number of Vertices n_v, Number of Symmetry-Distinct (N_S^{SD}) and Total (N_S) Face Spirals, Pentagon Neighboring Index N_P, Hexagon Strain Parameter σ_h, HOMO–LUMO Gap $\Delta\varepsilon_{HL}$ from a Hückel Analysis (in eV), Wiener Index W, and Szeged Index S_z of the Halma and Leapfrog Transforms of C_{364} and C_{366}

(k,l)	$t(k,l)$	n_v	N_S^{SD}	N_S	N_P	σ_h	$\Delta\varepsilon_{HL}$	W	S_z
				$T_{k,l}^{GC}(T\text{-}C_{364})$					
(1,0)	1	364	18	216	0	0.7115	0	778866	15215328
(1,1)	2	1092	5	60	0	0.3154	0.485	12186666	439133076
(2,0)	4	1456	25	300	0	0.2767	0	25023132	1044274308
(2,2)	12	4368	5	60	0	0.1638	0.243	390430080	29031693144
(3,0)	9	3276	41	492	0	0.1884	0.281	190158018	12165385368
(3,3)	27	9828	5	60	0	0.1099	0.162	2965469358	334243178292
(4,0)	16	5824	61	732	0	0.1423	0	801528588	69114647592
(4,4)	48	17472	5	60	0	0.0826	0.121	12497408760	606824313414
(5,0)	25	9100	85	1020	0	0.1142	0	2446359618	265400741868
(6,0)	36	13104	113	1356	0	0.0953	0.140	6087715572	795970632660
(7,0)	49	17836	145	1740	0	0.0818	0	13158459978	2013421949184
				$T_{k,l}^{GC}(D_3\text{-}C_{366})$					
(1,0)	1	366	57	342	6	0.7398	0.235	794568	16091457
(1,1)	2	1098	196	1176	0	0.3788	0.678	12405813	440654361
(2,0)	4	1464	70	420	0	0.3047	0.079	25477143	1046910918
(2,2)	12	4392	266	1596	0	0.1634	0.317	397278072	28568886036
(3,0)	9	3294	175	1050	0	0.1879	0.371	193538835	11997453945
(3,3)	27	9882	902	5412	0	0.1096	0.203	3017221629	326798431890
(4,0)	16	5856	54	324	0	0.1419	0.001	815676747	67618674624
(4,4)	48	17568	639	3834	0	0.0820	0.149	12715128384	1840123932168
(5,0)	25	9150	386	2316	0	0.1139	0	2489397258	258424188237
(6,0)	36	13176	240	1440	0	0.0951	0.174	6194618766	772638775344
(7,0)	49	17934	685	4110	0	0.0816	0	13389275154	1950026430255

polyhedron formula. They can, however, differ in their number of hexagons. In patches that contain at most one pentagon, the number of hexagons is uniquely defined by their boundary, i.e., vertex insertions can only be performed by replacing patches that contain at least two pentagons.[24,25] Two hexagon-only patches with the same boundary are, however, only guaranteed to be isomorphic if they consist of no more than 24 vertices.[26,24]

In the case of a constant number of hexagons, a patch replacement is formally an isomerization. Notable examples are the Stone–Wales transformation[23] and the generalized Stone–Wales transformation.[27,28] Formal isomerizations can be represented as the application of two-switches to a limited domain of the graph. According to Berge's switching theorem,[29,30] every fullerene graph of a given size can be derived from one isomer of the same size by consecutive two-switches.

In the case of a differing hexagon count, the transformation is called a formal vertex insertion or deletion. The first described examples are the Endo–Kroto two-vertex insertion,[31] Yoshida–Fowler four-vertex insertion,[32] and Yoshida–Fowler six-vertex insertion.[32] Brinkmann et al. compiled extensive lists of formal isomerizations[20] and formal vertex insertions/deletions.[21]

According to Hasheminezhad et al.,[33] every fullerene can be derived from either C_{20} or T_d-C_{28} by applying a sequence of vertex insertions. These vertex insertions (also referred to as "growth operations") are divided into three classes, two of which are of countably infinite size. Hence, as every fullerene can be constructed from C_{20} or T_d-C_{28} (which both admit a spiral), every nonspiralable fullerene can be derived from spiralable fullerenes by applying one or several vertex insertions.

More concretely, the substitution of one patch of vertices for another containing less vertices can be understood as the truncation of a domain of high curvature in the corresponding polyhedron. The curvature (which must always sum to $4\pi = 12 \times \pi/3$ in total) is thereby spread, and the distance between some or all pentagons involved increases. Vice versa, the addition of vertices resembles the capping of one or several faces. As a result, the distance between pentagons in the replaced patch decreases. It is not possible to truncate or cap a domain that contains one or no pentagon. The property of not having a face spiral is a global property of a fullerene graph and cannot be related to a specific subgraph. However, failing spirals typically fail at domains of high curvature, i.e., a subgraph that contains many pentagons in close proximity.

The NS-fullerenes T-C_{380} and D_3-C_{384} can be constructed by subsequent Yoshida–Fowler four-vertex (YF4) insertions[32] and Brinkmann–Fowler six-vertex (BF6) (denoted as G4.14.4.1 ↔ G4.14.2.2 by Brinkmann et al.) insertions,[21] respectively, as shown in eq 1.

$$T\text{-}C_{364} \xrightarrow{YF4} C_3\text{-}C_{368} \xrightarrow{YF4} C_2\text{-}C_{372} \xrightarrow{YF4} C_3\text{-}C_{376} \xrightarrow{YF4} T\text{-}C_{380}$$
$$D_3\text{-}C_{366} \xrightarrow{BF6} C_2\text{-}C_{372} \xrightarrow{BF6} C_2\text{-}C_{378} \xrightarrow{BF6} D_3\text{-}C_{384} \quad (1)$$

The DFT optimized structures of T-C_{364} and D_3-C_{366}, from which T-C_{380} and D_3-C_{384} are constructed, are shown in Figure 5. The corresponding face-spiral pentagon indices are listed in Table 1. T-C_{364} has no pentagon start for a face spiral, whereas D_3-C_{366} does. From Table 2, we also see that D_3-C_{366} admits more face spirals compared to T-C_{364}. All fullerenes leading to D_3-C_{384} by Brinkmann–Fowler six-vertex insertions have face spirals starting at a pentagon, while the ones leading to T-C_{380} by Yoshida–Fowler four-vertex insertions have no pentagon start.

dx.doi.org/10.1021/ci4005578 | J. Chem. Inf. Model. 2014, 54, 121–130

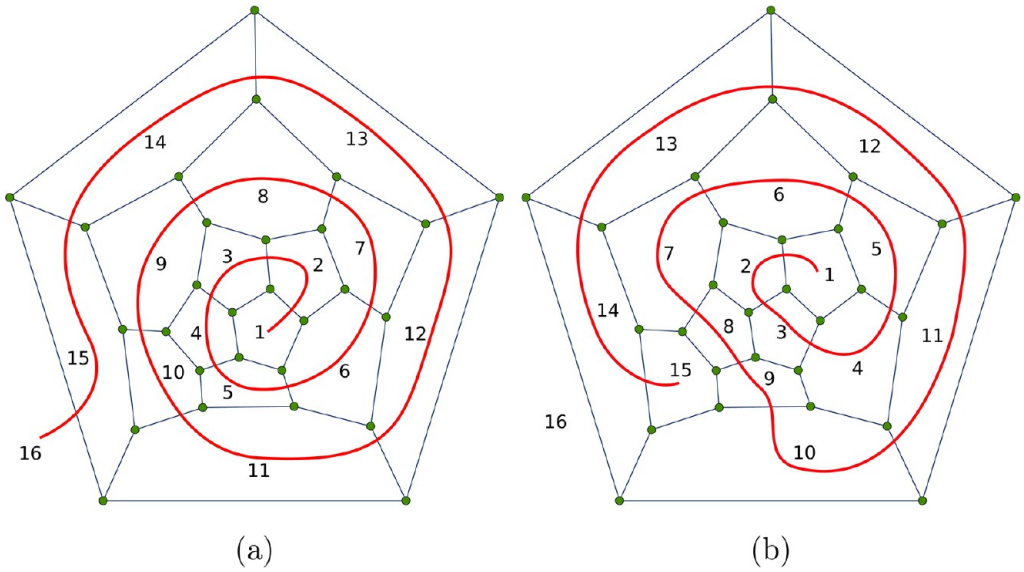

Figure 6. Two attempts to construct a spiral in the D_2 isomer of C_{28}: (a) succeeds while (b) misses face 16.

Construction of NS-Fullerenes through a Generalized Face Spiral. NS-fullerenes can only practically be found through an extensive search through all possible isomers by using efficient algorithms such as the Brinkmann−Goedgebeur−McKay patch replacement algorithm.[6,8] Once an NS-fullerene has been found, it can be completely characterized by a generalized face-spiral algorithm, which we will describe in this section.

The MF face-spiral algorithm was the first algorithm for creating fullerene graphs of a given size.[1,2] Furthermore, it offers a short and unambiguous description of fullerene graphs. It works as follows. In the dual of the cubic graph (which is a triangulation of the sphere), three vertices that are mutually connected, i.e., form a face, are chosen as a starting sequence. The remaining vertices are then added one-by-one, such that the next vertex is connected to the previous one and to the vertex that has been added earliest and which has open valencies left. By this procedure, a spiral that contains all vertices of the triangulation—corresponding to the faces of the cubic graph—is obtained. In other words, a face spiral in a fullerene is identical to a Hamiltonian spiral path for the fullerene dual. Giving the degree of the vertices (5 or 6 in the case of fullerene graphs) in the order in which they are added to the spiral, uniquely describes the graph. The spiral displayed in Figure 6(a) is denoted as "5555565665655555". This can be abbreviated by listing the positions of the 12 pentagons only. The aforementioned spiral would then be described by "1,2,3,4,5,7,10,12,13,14,15,16". The graph can unambiguously be reconstructed from this sequence.

The original face-spiral algorithm has the shortcoming that in some fullerene graphs there are starting sequences that lead to a failing spiral, i.e., there is a step in the spiral generation where the previous vertex and the vertex that has been added earliest and which has open valencies left do not have a common neighbor in the set of remaining vertices. In these cases, the spiral fails (Figure 6(b)). There are fullerene graphs in which *all* starting sequences lead to failing spirals.[3,34] These cannot be generated or described using the original face-spiral algorithm.

An extended version of the original MF face-spiral algorithm that we implemented recently into program *Fullerene* eliminates this shortcoming (similar generalized spiral codes have also been proposed by Brinkmann[35] and Fowler and co-workers[22]). During the spiral generation, a walk that traverses the boundary of the subgraph induced by the vertices that have been added to the spiral is maintained. The next vertex to be added is chosen as the vertex in the remaining subgraph that is adjacent to the first and the last vertex in the boundary walk (which is equivalent to the previous criterion). Before adding that vertex, however, it is checked whether the subgraph induced by the set of vertices that have not been added to the spiral yet remains connected after removing it. If this is not the case, a *jump*, i.e., a cyclic shift, is performed on the walk. The smallest offset that allows for adding a vertex to the spiral without disconnecting the remaining subgraph is chosen.

By demanding that the remaining subgraph must always remain connected, we ensure that the spiral never gets stuck, and hence, every fullerene graph can be constructed and described with a general spiral string. As we prove in a forthcoming paper, this algorithm is guaranteed to work for all connected planar cubic graphs.

The general pentagon indices are denoted as $n_1,k_1,...,n_m,k_m;p_1,...,p_{12}$, where n_i,k_i are the positions at which a jump is performed and the respective offset, and p_i are the positions of the 12 pentagons. Counting jump- and pentagon-positions starts from 1. If the jump list is empty, we omit the semicolon. The general spiral code describing the spiral in Figure 7(b) is "14,1;1,2,3,5,8,9,11,12,13,14,15,16", where n_1,k_1 = 14,1 indicates that a cyclic shift of length 1 is performed before adding face 14.

We define the canonical general spiral of a graph as the shortest of the $6n_v$ spiral codes (where n_v is the number of vertices in the cubic graph). If there is more than one shortest spiral code, the lexicographically smallest is chosen. Equations 2−5 list the canonical general spiral codes of the fullerene graphs that are investigated in this paper.

C_{380}: 110, 2; 45, 70, 71, 82, 83, 110, 119, 120, 144, 184, 185, 192 (2)

C_{384}: 49, 1; 29, 30, 31, 49, 145, 146, 170, 171, 190, 191, 192, 194 (3)

C_{440}: 62, 1; 39, 40, 41, 62, 170, 171, 197, 198, 218, 219, 220, 222 (4)

C_{672}: 142, 1; 51, 53, 109, 111, 220, 252, 288, 302, 304, 306, 320, 338 (5)

dx.doi.org/10.1021/ci4005578 | J. Chem. Inf. Model. 2014, 54, 121−130

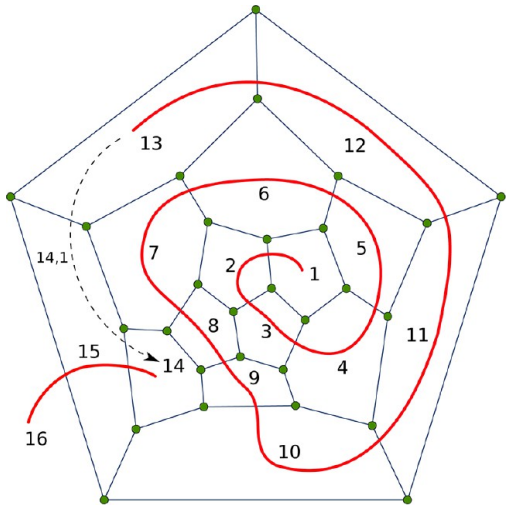

Figure 7. General spiral starting at the same position as the failing spiral in Figure 6(b).

Electronic Structure, Stability, and Geometry of NS-Fullerenes. The smallest NS-fullerene T-C_{380} has a large HOMO−LUMO gap of $\Delta\varepsilon_{HL}$ = 0.434 eV obtained from a Hückel analysis (Table 3). This compares well with the DFT calculations, which give 0.289 eV at the PBE and 0.640 eV at the B3LYP level of theory (the larger gap for the latter functional comes from the exact exchange contribution). D_3-C_{440} has a HOMO−LUMO gap of 0.055 eV, as shown in Table 4. In contrast, D_3-C_{384} and D_3-C_{672} have a zero gap and should undergo a first-order Jahn−Teller distortion into C_2 symmetry (active E-mode). Structurally, these Jahn−Teller distortions are extremely small for such large fullerenes and not visible to the naked eye. For example, for D_3-C_{384}, the optimized distances around the three bonds sharing two pentagons where the C_2-axes are situated are 1.4567, 1.4567, and 1.4570 Å (at the optimized B3LYP level of theory). In D_3-symmetry, these distances are all equal. However, the DFT calculations show an increased HOMO−LUMO gap of 0.291 eV for D_3-C_{384} using the PBE functional as compared to simple Hückel theory.

Concerning the stability of these fullerenes, we can compare to C_{60} by using the following (hypothetical) reaction, which approximates the energy difference per atom

$$\frac{1}{60}C_{60} \rightarrow \frac{1}{N}C_N + \Delta E_N \quad (6)$$

The results together with some other useful information of the optimized DFT structures are shown in Table 5. Figure 8 shows the stability of the four NS-fullerenes compared to a selection of the most stable fullerenes within a series of isomers from C_{20} to C_{540}. Here ΔE_N is plotted against $N^{-1/2}$ in order to extrapolate to the graphene limit ($N \rightarrow \infty$). We note in passing that in cluster physics a $N^{-1/3}$ behavior is chosen for compact 3D clusters to extrapolate to the solid state. This well-known behavior is derived for example from a liquid-drop model expansion of the free energy.[36,37] For fullerenes, the atoms are on the surface of a "sphere", which more realistically points toward a $N^{-1/2}$ behavior. Indeed, this law gives a much better correlation with the calculated ΔE_N values and is therefore applied here.

We first see that the fullerenes separate into two distinct sets, $C_{N<60}$ and $C_{N\geq 60}$ for the most stable fullerenes, the latter fulfilling the isolated pentagon rule (IPR). This results in two stability lines. Second, for the most stable IPR fullerenes, one obtains the graphene limit at −13 kcal/mol, in reasonable agreement with the estimated value of −9 kcal/mol obtained from heat of formation of graphite and considering the van der Waals interaction between graphene layers.[38,39] Third, the results show that the NS-fullerenes are reasonably stable with a destabilization of less than 2 kcal/mol per C−C bond compared to the most stable IPR fullerenes. The PBE and B3LYP results are very similar.

Table 5 contains many other useful properties. We see that T-C_{364} and its Yoshida−Fowler vertex inserted T-C_{380} have very similar volumes and surface areas (trivially the surface area increases from T-C_{364} to T-C_{380}) and so do D_3-C_{366} and D_3-C_{384}. However, a fullerene with a larger number of vertices does not have to be larger in size due to their completely different geometry, as shown by a comparison, for example, between T-C_{364} and D_3-C_{384}. Except for C_{60}, all fullerenes listed in Table 5 are slightly nonconvex, as shown by the (surface) convexity parameter $C_A = A_{CH}/A$. Here, A is the surface area of the fullerene, and A_{CH} the surface area of its convex hull. The nonconvexity of the fullerenes is clearly visible in Figures 1−5, where we see a slight concave curvature around the hexagons. The last three columns in table 5 measure the deviance for each fullerene from the ideal 3D sphere (for a detailed discussion see ref 9).

Table 3. Goldberg−Coxeter indices (k,l), Triangulation Parameter $t(k,l)$, Number of Vertices n_v, Number of Symmetry-Distinct (N_S^{SD}) and Total (N_S) Face Spirals, Pentagon Neighboring Index N_P, Hexagon Strain Parameter σ_h, HOMO−LUMO Gap $\Delta\varepsilon_{HL}$ from a Hückel Analysis (in eV), Wiener Index W, and Szeged Index S_z of the Halma and Leapfrog Transforms of C_{380}

(k,l)	$t(k,l)$	n_v	N_S^{SD}	N_S	N_P	σ_h	$\Delta\varepsilon_{HL}$	W	S_z
					$T_{k,l}^{GC}(T\text{-}C_{380})$				
(1,0)	1	380	0	0	12	0.5416	0.434	864762	17592456
(1,1)	3	1140	0	0	0	0.4259	0.428	13513974	493757544
(2,0)	4	1520	0	0	0	0.3250	0.290	27753252	1186112880
(2,2)	12	4560	0	0	0	0.1604	0.206	432893046	32677809552
(3,0)	9	3420	0	0	0	0.1845	0.238	210864450	13744636896
(3,3)	27	10260	0	0	0	0.1076	0.134	3287907642	376364250888
(4,0)	16	6080	0	0	0	0.1393	0.135	888748116	77890894116
(4,4)	48	18240	0	0	0	0.0809	0.099	13856139156	2126356677840
(5,0)	25	9500	0	0	0	0.1118	0.115	2712479754	298658043336
(6,0)	36	13680	0	0	0	0.0933	0.115	6749836440	894840528456
(7,0)	49	18620	0	0	0	0.0800	0.080	14589471486	2261961454188

dx.doi.org/10.1021/ci4005578 | J. Chem. Inf. Model. 2014, 54, 121−130

Table 4. Goldberg−Coxeter Indices (k,l), Triangulation Parameter $t(k,l)$, Number of Vertices n_v, Number of Symmetry-Distinct (N_S^{SD}) and Total (N_S) Face Spirals, Pentagon Neighboring Index N_P, Hexagon Strain Parameter σ_h, HOMO−LUMO Gap $\Delta\varepsilon_{HL}$ from a Hückel Analysis (in eV), Wiener Index W, and Szeged Index S_z of the Halma and Leapfrog Transforms of C_{384}, C_{440}, and C_{672}

(k,l)	$t(k,l)$	n_v	N_S^{SD}	N_S	N_P	σ_h	$\Delta\varepsilon_{HL}$	W	S_z
					$T_{k,l}^{GC}(D_3\text{-}C_{384})$				
(1,0)	1	384	0	0	15	0.5191	0	900972	18489834
(1,1)	3	1152	70	420	0	0.4481	0.769	14063379	503477097
(2,0)	4	1536	0	0	0	0.3354	0	28880766	1196989728
(2,2)	12	4608	8	48	0	0.1596	0.350	450300945	32482982520
(3,0)	9	3456	0	0	0	0.1836	0.411	219381558	13686989061
(3,3)	27	10368	178	1068	0	0.1071	0.220	3419854512	371063413764
(4,0)	16	6144	0	0	0	0.1386	0	924571380	77056229226
(4,4)	48	18432	0	0	0	0.0805	0.158	14411798937	2087919325548
(5,0)	25	9600	0	0	0	0.1112	0	2821708806	294297617166
(6,0)	36	13824	0	0	0	0.0928	0.186	7021504974	879481127910
(7,0)	49	18816	0	0	0	0.0796	0	15176486088	777771569091
					$T_{k,l}^{GC}(D_3\text{-}C_{440})$				
(1,0)	1	440	0	0	15	0.4866	0.055	1267804	27865848
(1,1)	3	1320	19	114	0	0.4196	0.736	19785768	757459407
(2,0)	4	1760	0	0	0	0.3142	0	40628424	1800847608
(2,2)	12	5280	0	0	0	0.1493	0.335	633463320	48809068236
(3,0)	9	3960	0	0	0	0.1718	0.392	308602644	20579946951
(3,3)	27	11880	0	0	0	0.1001	0.209	4810808520	557305601235
(4,0)	16	7040	0	0	0	0.1296	0.004	1300566284	115828515936
(4,4)	48	21120	0	0	0	0.0752	0.150	20273362905	3135159889380
(5,0)	25	11000	0	0	0	0.1040	0.0002	3969179866	442300731228
(6,0)	36	15840	0	0	0	0.0867	0.177	9876814590	1321616670198
(7,0)	49	21560	0	0	0	0.0744	0.002	21347979990	3334263250641
					$T_{k,l}^{GC}(D_3\text{-}C_{672})$				
(1,0)	1	672	0	0	0	0.4921	0	3632139	100189002
(1,1)	3	2016	194	1164	0	0.2377	0.474	56675358	2734390758
(2,0)	4	2688	0	0	0	0.2073	0	116374455	6513298290
(2,2)	12	8064	463	2778	0	0.1212	0.223	1814461428	177071344866
(3,0)	9	6048	0	0	0	0.1397	0.262	883922250	74585962914
(3,3)	27	18144	1116	6696	0	0.0811	0.145	13779758694	2024937702174
(4,0)	16	10752	0	0	0	0.1052	0	3725140125	420195517416
(4,4)	48	32256	1662	9972	0	0.0609	0	58069545396	11399985523686
(5,0)	25	16800	0	0	0	0.0843	0	11368648473	1605503429328
(6,0)	36	24192	0	0	0	0.0703	0	28289407236	4799169761892
(7,0)	49	32928	0	0	0	0.0603	0	61145300079	12111032215788

Table 5. Properties Obtained from DFT Optimizations[a]

fullerene	DFT	r_{min}	r_{max}	r_{MCS}	ΔE_N	V	A	C_A	q_{IPQ}	D_{MDS}	λ_{asym}
I_h-C_{60}	PBE	1.407	1.457	3.565	0	164.8	150.3	1.0000	0.904	0.0	0.0
	B3LYP	1.398	1.455	3.555	0	163.3	149.4	1.0000	0.904	0.0	0.0
T-C_{364}	PBE	1.398	1.457	11.30	−6.002	2432.2	959.3	1.0157	0.758	15.05	7.449
	B3LYP	1.388	1.454	11.25	−6.351	2408.2	952.7	1.0157	0.758	15.02	7.429
D_3-C_{366}	PBE	1.400	1.463	13.96	−5.155	2119.4	964.5	1.0434	0.566	40.74	26.65
	B3LYP	1.393	1.462	13.90	−5.445	2100.0	958.0	1.0436	0.567	40.52	26.57
T-C_{380}	PBE	1.411	1.462	12.82	−5.430	2487.4	1001.5	1.0260	0.697	17.60	10.84
	B3LYP	1.404	1.461	12.77	−5.712	2462.8	994.7	1.0205	0.697	17.52	10.82
D_3-C_{384}	PBE	1.396	1.464	15.73	−4.724	2183.1	1012.1	1.0635	0.520	44.95	33.62
	B3LYP	1.386	1.462	15.68	−4.978	2162.9	1005.3	1.0632	0.521	44.62	33.53
D_3-C_{440}	PBE	1.407	1.493	16.98	−5.124	2661.8	1161.2	1.0706	0.512	47.72	39.74
	B3LYP	1.387	1.465	17.01	−5.399	2637.7	1153.2	1.0672	0.513	47.40	39.63
D_3-C_{672}	PBE	1.399	1.465	18.89	−6.814	5307.2	1779.0	1.0298	0.566	42.03	49.38
	B3LYP	1.390	1.465	18.82	−7.249	5260.0	1766.9	1.0301	0.567	41.79	49.18

[a]Smallest (r_{min}) and largest bond distance (r_{max}) in Å, radius of minimum covering sphere r_{MCS} in Å, energetic stability ΔE_N per carbon atom compared to C_{60} in kcal/mol as defined in eq 6, volume V in Å^3 and surface area A in Å^2, convexity parameter C_A, isoperimetric quotient q_{IPQ}, spherical distortion parameter from minimum distance sphere D_{MDS} in %, and Fowler asymmetry parameter λ_{asym}.

dx.doi.org/10.1021/ci4005578 | J. Chem. Inf. Model. 2014, 54, 121−130

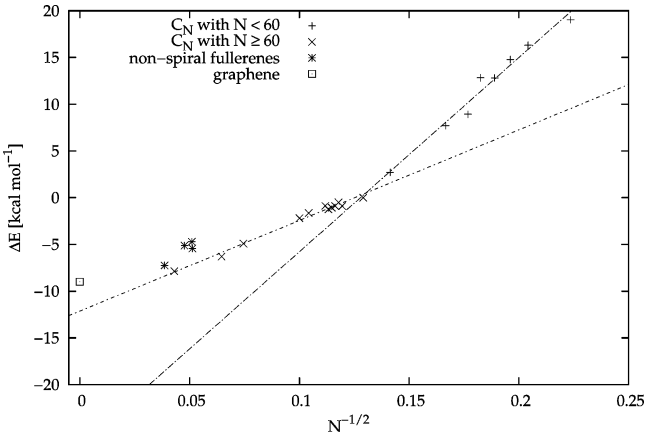

Figure 8. Stability of NS-Fullerenes compared to C_{60}, i.e., $E(C_N)/N - E(C_{60})/60$ (in kcal/mol), with E being the total electronic energy. For the two lines, the most stable fullerenes have been chosen, i.e., IPR fullerenes for $N > 60$. The stabilities of the IPR fullerenes are extrapolated linearly to the graphene limit.

HALMA AND LEAPFROG TRANSFORMS OF NS-FULLERENES

The Goldberg–Coxeter transformation,[10,11] $T^{GC}_{k,l}$, transforms a fullerene with vertex number $n_v = N$ to a larger fullerene with $n_v = N(k^2 + kl + l^2)$ [$t(k,l) = (k^2 + kl + l^2)$ is called the triangulation number] with the same shape and symmetry.[2] Two particularly simple GC transforms are the *halma* and *leapfrog* transformations, corresponding to $l = 0$ and $k = l$, respectively. We call the $l = 0$ case, which is shown in Figure 9(a), the "halma" transform due to the construction's similarity to a halma game board. It is also sometimes called a k-inflation. The leapfrog transformation is illustrated in Figure 9(b).

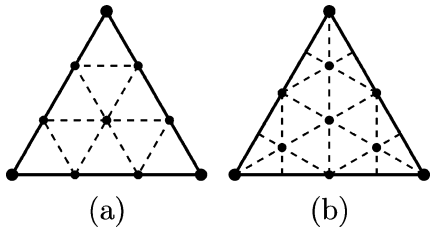

Figure 9. Two examples for the Goldberg Coxeter transformation: (a) the third halma transformation $T^{GC}_{3,0}$ and (b) the third leapfrog transformation $T^{GC}_{3,3}$.

We briefly mention some important properties of GC transformations. The GC transform can be described in terms of multiplication by complex numbers $(k + l\omega)$, where $\omega = e^{i2\pi/6}$, in what is called the *Eisenstein plane*.

Because of this, any number of GC transformations can be composed into a single GC transformation, corresponding to the product of the Eisenstein numbers, as follows

$$T^{GC}_{k_1,l_1} T^{GC}_{k_2,l_2} = T^{GC}_{k_1k_2 - l_1l_2, l_1k_2 + (k_1+l_1)l_2} \quad (7)$$

$T^{GC}_{1,0} = 1$ is the unit transformation. GC transformations commute with each other, i.e.,

$$T^{GC}_{k_1,l_1} T^{GC}_{k_2,l_2} = T^{GC}_{k_2,l_2} T^{GC}_{k_1,l_1} \quad (8)$$

The GC transform is 12-fold symmetric through the transformations

$$k + l\omega \rightarrow (k + l\omega)\omega^j \text{ for } j = 0, \ldots, 5$$
$$k + l\omega \rightarrow l + k\omega \quad (9)$$

From eq 7, we can derive the combined leapfrog and halma transformations

$$T^{GC}_{1,1} T^{GC}_{1,1} = (T^{GC}_{1,1})^2 = T^{GC}_{0,3} = T^{GC}_{3,0} \quad (10)$$

$$T^{GC}_{1,1} T^{GC}_{k,0} = T^{GC}_{k,k} \quad (11)$$

$$T^{GC}_{k,0} T^{GC}_{l,0} = T^{GC}_{kl,0} \quad (12)$$

Hence, we obtain all possible GC transformations of the form $T^{GC}_{k,0}$ and $T^{GC}_{k,k}$ from such combinations as implemented in *Fullerene*. The two largest halma transforms of C_{380} and C_{384} studied here are shown in Figures 10 and 11.

Tables 3 and 4 list properties of the GC transforms of the four NS fullerenes studied. None of the halma transforms admit any ring spiral. This leads us to the following conjecture:

Conjecture. *Any halma transform of an NS-fullerene is also an NS-fullerene.*

If this conjecture is true, the class of NS-fullerenes is infinite, even though it is vanishingly small compared to the class of all fullerenes for the range where exhaustive search has been performed, and we expect it to be so for larger N as well.

In Tables 3 and 4, we see that many of the leapfrogged NS-fullerenes are NS-fullerenes themselves but that in general they are not. Brinkmann and Fowler have investigated spiralability of the leapfrogs of several million cubic polyhedra and found that these leapfrogs statistically are less likely to have spirals than their parents.[40]

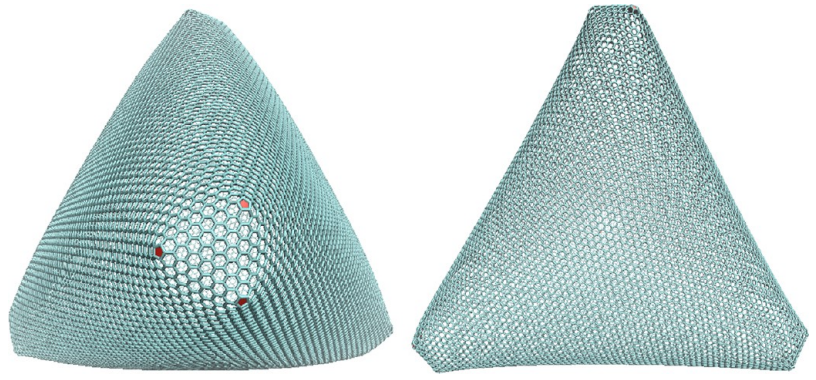

Figure 10. Force-field optimized structure of $T^{GC}_{7,0}[C_{380}] = C_{18620}$. View from the top (left) and side (right) of the polyhedron.

dx.doi.org/10.1021/ci4005578 | J. Chem. Inf. Model. 2014, 54, 121–130

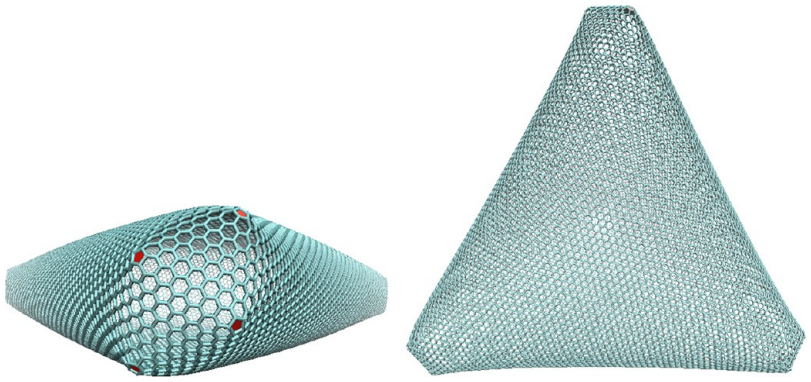

Figure 11. Force-field optimized structure of $T^{GC}_{7,0}[C_{384}] = C_{18816}$. View from the top (left) and side (right) of the polyhedron.

We see from Table 5 that a leapfrog of a spiralable fullerene can be either spiralable or nonspiralable. For example, $T^{GC}_{1,1}[C_{440}]$ admits a spiral, but $T^{GC}_{1,1}T^{GC}_{1,1}[C_{440}] = T^{GC}_{3,0}[C_{440}]$ does not. Similarly, the halma transform of a spiralable fullerene can be either; NS-D_3-C_{672} provides a counterexample to the spiralable fullerenes being closed under the halma transform because it can be written as the halma transform $T^{GC}_{2,0}[D_3\text{-}C_{168}]$.

The face-spiral pentagon indices for D_3-C_{168} are given in Table 1. As expected, the spiral count for the D_3-C_{168} fullerene is low, i.e., we get 11 distinct face spirals out of a total of only 66. NS-D_3-C_{672} is likely to be the smallest Goldberg−Coxeter NS-fullerene. We mention that the D_3-$C_{924} = T^{GC}_{3,40}[D_3\text{-}C_{308}]$ may well be the first leapfrog NS-fullerene.

For completion and future reference, we also list topological indicators (Wiener and Szeged index) for C_{364}, C_{366}, C_{380}, C_{384}, C_{440}, and C_{672} and their smallest Goldberg−Coxeter transforms for $l = 0$ or $l = k$ in Tables 2, 4, and 5.

CONCLUSIONS

We investigated the four NS-fullerenes, NS-T-C_{380}, NS-D_3-C_{384}, NS-D_3-C_{440}, and NS-D_3-C_{672}, as well as their leapfrog and halma transforms up to about 30,000 atoms. The NS-fullerenes were optimized and analyzed quantum chemically at the DFT level of theory, while the larger transformed fullerenes were force-field optimized and analyzed using graph theoretical methods.

NS-T-C_{380} has a large HOMO−LUMO gap of 0.434 eV, while C_{440}, C_{384}, and C_{672} have a small or zero gap, which places them among the semiconductors and conductors, respectively. The predicted Jahn−Teller distortion undergone by the zero gap fullerenes was found to be so minor as to be undetectable by visual inspection of the structure.

NS-fullerenes typically have clusters of pentagons in close proximity, leading to sharp curvature and reduced stability compared to more spherical fullerenes of equal size, but the investigated NS-fullerenes remain reasonably stable with less than 2 kcal/mol difference per bond to the icosahedral isomers. All four quantum chemically optimized geometries are found to be slightly concave, a feature that is predicted by the force-field optimization, showing that the concavity arises directly from the graph topology rather than the electronic structure.

It was found that the leapfrog transformation may introduce spiralability, while all the halma-transformed fullerenes were unspiralable. We conjecture that this class of NS-fullerenes is closed under the halma transform. However, the converse is not true; a counterexample is NS-C_{672}, which is the second halma transform of C_{168}.

While the vanishingly small proportion of isomers with no spirals makes it difficult to find examples of NS-fullerenes through extensive search, especially for large values of N, new NS-fullerenes can be obtained from existing ones through halma transformations if our proposed conjecture holds. Furthermore, we conclude that none of the investigated leapfrogs of NS-T-C_{380} are spiralable.

AUTHOR INFORMATION

Corresponding Author

*E-mail: p.a.schwerdtfeger@massey.ac.nz.

Notes

The authors declare no competing financial interest.

ACKNOWLEDGMENTS

P.S. is indebted to the Alexander von Humboldt Foundation (Bonn) for financial support in terms of a Humboldt Research Award at the Philipps University of Marburg. R.T. thanks the Humboldt foundation for support via an Alumni fellowship and the LOEWE-CSC Frankfurt for providing computational resources.

REFERENCES

(1) Manolopoulos, D. E.; May, J. C.; Down, S. E. Theoretical studies of the fullerenes: C_{34} to C_{70}. *Chem. Phys. Lett.* **1991**, *181*, 105−111.

(2) Fowler, P. W.; Manolopoulos, D. E. *An Atlas of Fullerenes*, 2nd ed.; Dover Publications, Inc.: Mineola, NY, 2006.

(3) Manolopoulos, D. E.; Fowler, P. W. A fullerene without a spiral. *Chem. Phys. Lett.* **1993**, *204*, 1−7.

(4) Fowler, P. W. Systematics of Fullerenes and Related Clusters. *Phil. Trans. R. Soc. Lond.* **1993**, *343*, 39−52.

(5) Yoshida, M.; Fowler, P. Systematic relationships between fullerenes without spirals. *Chem. Phys. Lett.* **1997**, *278*, 256−261.

(6) Brinkmann, G.; Goedgebeur, J.; Mélot, H.; Coolsaet, K. House of Graphs: A database of Interesting Graphs. *Discrete Appl. Math.* **2013**, *161*, 311−314.

(7) Brinkmann, G.; Goedgebeur, J.; Mélot, H.; Coolsaet, K. House of Graphs: a Database of Interesting Graphs, 2013. http://hog.grinvin.org (accessed December 8, 2013).

(8) Brinkmann, G.; Goedgebeur, J.; McKay, B. D. The generation of fullerenes. *J. Chem. Inf. Model.* **2012**, *52*, 2910−2918.

(9) Schwerdtfeger, P.; Wirz, L.; Avery, J. Program fullerene: A software package for constructing and analyzing structures of regular fullerenes. *J. Comput. Chem.* **2013**, *34*, 1508−1526.

(10) Goldberg, M. A class of multi-symmetric polyhedra. *Tohoku Math. J.* **1937**, *43*, 104−108.

(11) Dutour, M.; Deza, M. Goldberg−Coxeter construction for 3- and 4-valent plane graphs. *J. Combinatorics* **2004**, *11*, 1−49.

(12) Tutte, W. T. How to draw a graph. *Proc. London Math. Soc.* **1963**, *13*, 743−767.
(13) Perdew, J. P.; Burke, K.; Ernzerhof, M. Generalized gradient approximation made simple. *Phys. Rev. Lett.* **1996**, *77*, 3865−3868.
(14) Becke, A. D. Density-functional thermochemistry. III. The role of exact exchange. *J. Chem. Phys.* **1993**, *98*, 5648−5652.
(15) Lee, C.; Yang, W.; Parr, R. G. Development of the Colic−Salvetti correlation-energy formula into a functional of the electron density. *Phys. Rev. B* **1988**, *37*, 785−789.
(16) Weigend, F.; Ahlrichs, R. Balanced basis sets of split valence, triple zeta valence and quadruple zeta valence quality for H to Rn: Design and assessment of accuracy. *Phys. Chem. Chem. Phys.* **2005**, *7*, 3297−3305.
(17) Weigend, F. Accurate Coulomb-fitting basis sets for H to Rn. *Phys. Chem. Chem. Phys.* **2006**, *8*, 1057−1065.
(18) Ahlrichs, R.; Bär, M.; Häser, M.; Horn, H.; Kölmel, C. Electronic structure calculations on workstation computers: the program system TURBOMOLE. *Chem. Phys. Lett.* **1989**, *162*, 165−169.
(19) Frisch, M. J.; Trucks, G. W.; Schlegel, H. B.; Scuseria, G. E.; Robb, M. A.; Cheeseman, J. R.; Scalmani, G.; Barone, V.; Mennucci, B.; Petersson, G. A.; Nakatsuji, H.; Caricato, M.; Li, X.; Hratchian, H. P.; Izmaylov, A. F.; Bloino, J.; Zheng, G.; Sonnenberg, J. L.; Hada, M.; Ehara, M.; Toyota, K.; Fukuda, R.; Hasegawa, J.; Ishida, M.; Nakajima, T.; Honda, Y.; Kitao, O.; Nakai, H.; Vreven, T.; Montgomery, J. A., Jr.; Peralta, J. E.; Ogliaro, F.; Bearpark, M.; Heyd, J. J.; Brothers, E.; Kudin, K. N.; Staroverov, V. N.; Kobayashi, R.; Normand, J.; Raghavachari, K.; Rendell, A.; Burant, J. C.; Iyengar, S. S.; Tomasi, J.; Cossi, M.; Rega, N.; Millam, J. M.; Klene, M.; Knox, J. E.; Cross, J. B.; Bakken, V.; Adamo, C.; Jaramillo, J.; Gomperts, R.; Stratmann, R. E.; Yazyev, O.; Austin, A. J.; Cammi, R.; Pomelli, C.; Ochterski, J. W.; Martin, R. L.; Morokuma, K.; Zakrzewski, V. G.; Voth, G. A.; Salvador, P.; Dannenberg, J. J.; Dapprich, S.; Daniels, A. D.; Farkas, Ö.; Foresman, J. B.; Ortiz, J. V.; Cioslowski, J.; Fox, D. J. Gaussian 09, Revision C.1. Gaussian, Inc.: Wallingford CT, 2009.
(20) Brinkmann, G.; Fowler, P. W.; Justus, C. A catalogue of isomerization transformations of fullerene polyhedra. *J. Chem. Inf. Comput. Sci.* **2003**, *43*, 917−927.
(21) Brinkmann, G.; Fowler, P. W. A catalogue of growth transformations of fullerene polyhedra. *J. Chem. Inf. Comput. Sci.* **2003**, *43*, 1837−1843.
(22) Fowler, P. W.; Graovac, A.; Žerovnik, J.; Pisanski, T. *A Generalized Ring Spiral Algorithm for Coding Fullerenes and Other Cubic Polyhedra*; Preprint Series; Institute of Mathematics, Physics and Mechanics, Department of Mathematics, University of Ljubljana: Slovenia, 1998.
(23) Stone, A. J.; Wales, D. J. Theoretical studies of icosahedral C_{60} and some related species. *Chem. Phys. Lett.* **1986**, *128*, 501−503.
(24) Brinkmann, G.; Graver, J. E.; Justus, C. Numbers of faces in disordered patches. *J. Math. Chem.* **2009**, *45*, 263−278.
(25) Graver, J. E.; Graves, C. M. Fullerene patches I. *Ars Math. Contemp.* **2010**, *3*, 109−120.
(26) Guo, X.; Hansen, P.; Zheng, M. Boundary uniqueness of fusenes. *Discrete Appl. Math.* **2002**, *118*, 209−222.
(27) Balaban, A. T.; Schmalz, T. G.; Zhu, H.; Klein, D. J. Generalizations of the Stone−Wales rearrangement for cage compounds, including fullerenes. *J. Mol. Struct (THEOCHEM)* **1996**, *363*, 291−301.
(28) Ori, O.; Cataldo, F.; Putz, M. V. Topological anisotropy of Stone−Wales waves in graphenic fragments. *Int. J. Mol. Sci.* **2011**, *12*, 7934−7949.
(29) Berge, C. *Graphs and Hypergraphs*; Elsevier, New York, 1973.
(30) Ori, O.; Putz, M. V.; Gutman, I.; Schwerdtfeger, P. Generalized Stone−Wales Transformations for Fullerene Graphs Derived from Berge's Switching Theorem. In *Ante Graovac - Life and Works*; Gutman, I., Pokric, B., Vukicevic, D., Eds.; Mathematical Chemistry Monographs; University of Kragujevac: Kragujevac, Serbia, 2014; Vol. *16*; pp 259−272.
(31) Endo, M.; Kroto, H. W. Formation of carbon nanofibers. *J. Phys. Chem.* **1992**, *96*, 6941−6944.
(32) Yoshida, M.; Fowler, P. W. Systematic relationships between fullerenes without spirals. *Chem. Phys. Lett.* **1997**, *278*, 256−261.
(33) Hasheminezhad, M.; Fleischner, H.; McKay, B. D. A universal set of growth operations for fullerenes. *Chem. Phys. Lett.* **2008**, *464*, 118−121.
(34) Brinkmann, G.; Goedgebeur, J.; McKay, B. D. The smallest fullerene without a spiral. *Chem. Phys. Lett.* **2012**, *522*, 54−55.
(35) Brinkmann, G. Problems and scope of spiral algorithms and spiral codes for polyhedral cages. *Chem. Phys. Lett.* **1997**, *272*, 193−198.
(36) Brack, M. The physics of simple metal clusters: Self-consistent jellium model and semiclassical approaches. *Rev. Mod. Phys.* **1993**, *65*, 677−732.
(37) Tonner, R.; Frenking, G.; Lein, M.; Schwerdtfeger, P. Packed to the rafters: Filling up C_{60} with rare gas atoms. *ChemPhysChem* **2011**, *12*, 2081−2084.
(38) Beckhaus, H.-D.; Rüchardt, C.; Kao, M.; Diederich, F.; Foote, C. S. The Stability of buckminsterfullerene (C_{60}): Experimental determination of the heat of formation. *Angew. Chem., Int. Ed.* **1992**, *31*, 3−64.
(39) Dappe, Y. J.; Basanta, M. A.; Flores, F.; Ortega, J. Weak chemical interaction and van der Waals forces between graphene layers: A combined density functional and intermolecular perturbation theory approach. *Phys. Rev. B* **2006**, *74*, 205434−1−9.
(40) Brinkmann, G.; Fowler, P. W. Spiral coding of leapfrog polyhedra. *J. Chem. Inf. Comput. Sci.* **1998**, *38*, 463−468.